University of Massachusetts Amherst

ScholarWorks@UMass Amherst

2009

Nonisotropy in the CMB power spectrum in single field inflation

JF Donoghue
donoghue@physics.umass.edu

K Dutta

A Ross

Recommended Citation

Non-isotropy in the CMB power spectrum in single field inflation

John F. Donoghue[a] [1], Koushik Dutta[a,b] [2], Andreas Ross[a,c] [3],

[a] Department of Physics
University of Massachusetts
Amherst, MA 01003, USA

[b] Max-Planck-Institut für Physik (Werner-Heisenberg-Institut)
Föhringer Ring 6, D-80805 München, Germany

[c] Department of Physics
Yale University
New Haven, CT 06520, USA

Abstract

Contaldi *et al.* [1] have suggested that an initial period of kinetic energy domination in single field inflation may explain the lack of CMB power at large angular scales. We note that in this situation it is natural that there also be a spatial gradient in the initial value of the inflaton field, and that this can provide a spatial asymmetry in the observed CMB power spectrum, manifest at low values of ℓ. We investigate the nature of this asymmetry and comment on its relation to possible anomalies at low ℓ.

[1] E-mail: donoghue@physics.umass.edu
[2] E-mail: koushik@mppmu.mpg.de
[3] E-mail: andreas.ross@yale.edu

1   Introduction

The simplest models of inflation involve only a single scalar field, the inflaton [2]. With a suitably chosen potential, such a model can provide a simple explanation of the temperature fluctuations in the CMB at all angular scales [3]. There are however a number of possible anomalies in the CMB power spectrum that have attracted the attention of many researchers [4], [5], [6], [7], [8], [9], [10], [11], [12], [13], [14]. (However see also [15].) None of these anomalies is by itself statistically compelling; however, taken together they provide a hint that these features may be significant. Much discussion of anomalies involves the power spectrum at low ℓ, *i.e.* at large scales, where several anomalies indicate a possible spatial asymmetry in the power spectrum, most often roughly a north-south galactic coordinate asymmetry [4], [5], [6], [9], [11], [12], [13], [14].

The possibility that there may be an asymmetry in the observed CMB power spectrum was first raised by Eriksen *et al* [4] and Hansen *et al* [5] using the first year WMAP data. Their data analysis suggested a difference in power of roughly 20% for low ℓ maximized in the direction of galactic coordinates $(80°, 57°)$. Interestingly no effect was seen above $\ell \sim 40$. For example, the analysis of the power spectrum in the vicinity of the first acoustic peak [5, 16] showed no evidence of a spatial asymmetry. At low values of ℓ, the cosmic variance provides an intrinsic scatter in the power spectrum data, so that even though the signal is rather large, the statistical significance of their result was below 3 standard deviations.

In their three year data release [3], the WMAP team addressed the isotropy of the power spectrum, finding a small asymmetry in a direction consistent with Eriksen *et al* [4]. The method introduced by the WMAP team to investigate asymmetries in the CMB spectrum is to multiply an isotropic Gaussian CMB field by a large scale modulation function. They test both a dipole and a quadrupole modulation and find that the significance of the signal is not statistically compelling. Their analysis uses a pixel size of $7°$ which makes their analysis sensitive up to $\ell \sim 20$. The original Eriksen team has also revisited the WMAP 3 year data [9] using a statistical framework similar to the WMAP team's with a modulation function. They choose a higher resolution with a pixel size of $3.6°$ including multipoles up to $\ell \sim 40$ in their analysis and confirm the asymmetry with a higher statistical significance than the WMAP team and in consistency with their previous analysis of the first year WMAP data.

Hansen *et al* [11] and Maino *et al* [12] explored two different approaches to extract the CMB spectrum where WMAP data itself is used for foreground removal, and both find an asymmetry of the power spectrum at largest scales consistent with previous analysis and with each other. The fact that the asymmetry does not vary when different foreground subtraction procedures are applied constitutes a strong argument against a galactic origin for the asymmetry. Moreover, the asymmetry was also found in COBE data [4] which indicates that systematics may not be the correct explanation for a large scale asymmetry in the CMB power spectrum. Räth *et al* [13] have also found the asymmetry in the WMAP 3 year data using statistical techniques different from the ones used in previous analyses. Recent analyses of WMAP 5 year data show a similar anisotropy of power between the two hemispheres, but with the asymmetry possibly reaching to higher multipoles [14]. Otherwise, the nature of the asymmetry and the maximum asymmetry direction remains almost the same, and it will be interesting to see what results from Planck will have to say about an asymmetry at small scales.

These analyses provide motivations for the study of inflationary models that can generate a spatial asymmetry at low ℓ while remaining isotropic at larger values of ℓ. If these anomalies prove to be valid indicators of an asymmetry in the power spectrum, they can provide a direct probe of inflationary dynamics. Significant work that attempts to find a solution to these

anomalies has already appeared [17], [18], [19], [20] in the literature.

In this paper we discuss a simple situation that could lead to a spatial asymmetry in the CMB power spectrum at low values of ℓ within single field inflation. This involves an initial period of fast-roll expansion driven by the inflaton kinetic energy. The possibility of such an initial fast-roll period has been proposed by Contaldi, Peloso, Kofman and Linde (CPKL) [1] as a mechanism to explain the lack of CMB power at low ℓ. This mechanism provides a suppression of the spectrum of primordial perturbations and thus of the CMB at large scales, and it has also been worked on by others [21].

We will argue that in situations where the initial kinetic energy is significant in comparison to the potential energy, we should also expect the presence of a spatial gradient in the initial conditions of the inflaton field. We will show that even a surprisingly small value of an initial gradient – of order a few percent – will leave an observable spatial asymmetry in the CMB power spectrum at low ℓ. Essentially, the power suppression in the fast-roll model occurs at scales that depend sensitively on the initial magnitude of the scalar field in the frame where the kinetic energy is uniform and isotropic. This leads to a characteristic pattern for the spatial dependence of the power spectrum. While we will provide a brief discussion of two-field models below, we here focus on the single field fast-roll option because of its simplicity and predictive power.

2 Kinetic energy and spatial asymmetries

Inflation provides an explanation for the isotropy and homogeneity of the present universe. Rather than having to postulate extremely smooth initial conditions for the early universe, a long period of inflation will take non-smooth initial conditions and still lead to a highly isotropic and homogeneous observable universe today. However, if the number of e-foldings of inflation is just barely the minimal number, about 60, the initial conditions could be relevant and could modify the first few e-foldings.

The CPKL mechanism [1] postulates an initial period of kinetic energy dominance which then rapidly evolves into the standard slow-roll paradigm where the potential energy dominates and the universe inflates. If the slow-roll phase is many e-foldings longer than the minimum number of e-folds, the effects of the initial kinetic phase will be unobservable since the scales associated to its effects will be stretched far beyond our observable horizon. However, if the slow-roll phase is close to the minimum number of e-folds, then that initial kinetic phase will modify the first few e-foldings that generate the CMB power spectrum on largest scales, *i.e.* for small values of ℓ.

In a universe dominated by a uniform scalar field, the equations of motion are the Klein-Gordon equation on a FRW background

$$\ddot{\phi} + 3H\dot{\phi} + \frac{dV}{d\phi}(\phi) = 0 \tag{1}$$

and the Friedman equation[1]

$$H^2 = \left(\frac{\dot{a}}{a}\right)^2 = \frac{8\pi}{3}\rho = \frac{8\pi}{3}\left(\frac{\dot{\phi}^2}{2} + V(\phi)\right), \tag{2}$$

and the equation of state parameter is

$$w = \frac{P}{\rho} = \frac{\frac{\dot{\phi}^2}{2} - V(\phi)}{\frac{\dot{\phi}^2}{2} + V(\phi)}. \tag{3}$$

---

[1] We use units where $M_P = G^{-1/2} = 1$.

The CPKL assumption is an initial condition in which the inflaton velocity, $\dot{\phi}$, is non-zero and the kinetic energy term is dominant over the potential energy, $\frac{\dot{\phi}^2}{2} \gg V(\phi)$. During this initial phase $w \approx 1$ and the expansion of the universe will be decelerating similar to a matter dominated universe rather than a deSitter expansion. In this phase the kinetic energy rapidly decreases, until eventually the potential energy dominates and we enter the usual slow-roll phase. There is a short transitional phase when the potential energy already dominates and the universe inflates, but the inflaton velocity has not yet settled to its slow-roll value $\dot{\phi}_{SR} \simeq -\frac{1}{2\sqrt{6\pi}} \frac{dV}{d\phi}/V^{1/2}$.

The initial conditions involve specifying both ϕ and $\dot{\phi}$ which have to be chosen appropriately to obtain only about 60 e-folds of inflation so that the effects of the initial fast-roll stage are observable. CPKL then show that the quantum fluctuations are suppressed during the onset of inflation when the inflaton is fast-rolling – this will be reviewed in the next section. The picture that emerges then involves suppressed fluctuations at early times followed by standard slow-roll behavior. Since the earliest times correspond to the largest scales, the low ℓ multipoles are suppressed while the higher ones are standard.

Our extension of CPKL comes from the observation that the initial conditions in ϕ and $\dot{\phi}$ need not be the same at all positions in space. If they are close to uniform, one can expand the values in a multipole expansion. The first deviation from uniformity would consist of a gradient in the initial conditions across the initial patch. We will consider only such leading linear deviations from uniformity in this paper.

CPKL invoke a uniform initial condition in $\dot{\phi}$. Actually this is not a separate assumption. Because the value of $\dot{\phi}$ is changing with time, one can always choose a time-slicing such that $\dot{\phi}$ is uniform across the initial time slice. That is, if there is a gradient in the initial condition for $\dot{\phi}$ using one definition of the initial time slice, one can change to another definition such that this variable is uniform. However, in this frame there is no a priori reason for the initial value of the magnitude of ϕ itself to be uniform. A mechanism that can produce a temporal variation in ϕ can in principle also produce a spatial gradient in the field. We could equally well define a different time frame in which the initial condition of ϕ is uniform, but in this frame we would in general not expect that the initial value of $\dot{\phi}$ is constant in space. It is an extra assumption to assume that the initial conditions for ϕ and $\dot{\phi}$ are spatially uniform in the same frame.

We can obtain an invariant description of the evolution of the inflaton by considering trajectories in the $\phi - \dot{\phi}$ plane, displayed in Fig. 1 for a chaotic inflation potential $V(\phi) = \frac{1}{2}m^2\phi^2$. There are three phases visible in this plot: Initially, kinetic energy dominates and due to the rapid decrease in the kinetic energy, the trajectory runs quickly to the slow-roll attractor line where $\dot{\phi} \simeq \dot{\phi}_{SR} = const$. All initial trajectories are attracted to this line - this is one of the key features of inflation. Finally at the end of inflation, there is inflaton decay and reheating. However, different starting points lead to differing amounts of the slow-roll phase – these are shown as different initial trajectories. The number of e-folds of slow-roll inflation is

$$N \simeq 2\pi\phi_{SR,i}^2 \qquad (4)$$

where $\phi_{SR,i}$ is the field value when the phase space trajectory hits the slow-roll attractor.

If we start in a frame with a uniform value of ϕ, which would be represented by a vertical slice through the initial trajectories, one needs significantly different initial values of $\dot{\phi}$ in order to end up at different points on the slow-roll attractor. However, if we use a frame with uniform initial values of $\dot{\phi}$, which would be a horizontal slice through the trajectories, only a small difference in the initial values of ϕ are required to produce distinct trajectories with differing amounts of slow-roll behavior and thus differing amounts of inflation. We will
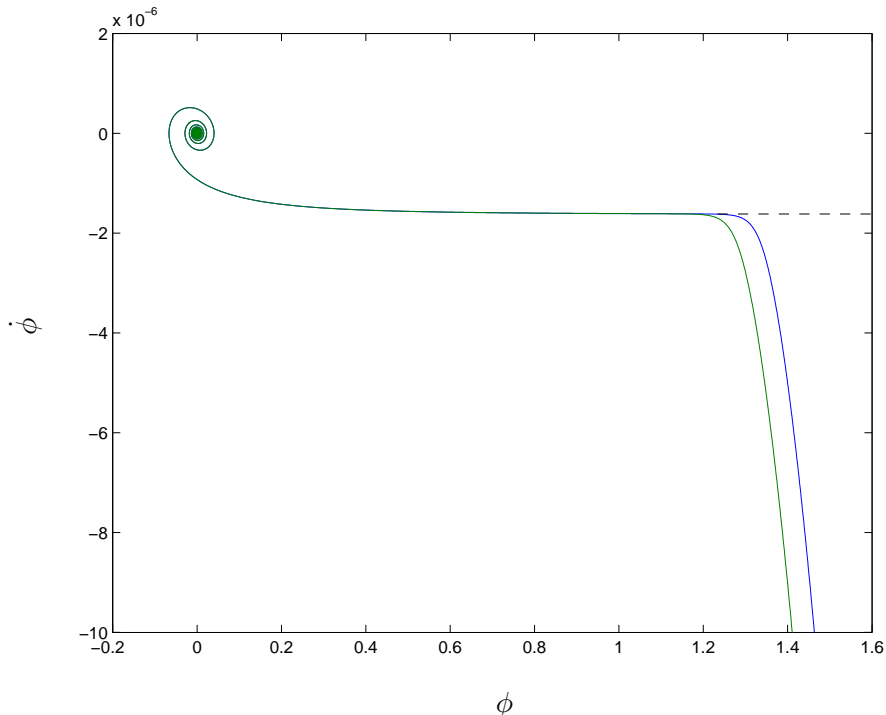
Figure 1: Phase space diagram of inflationary background solutions for two different values of the initial scalar field with both initially in the kinetic energy domination regime. The dashed curve shows the slow-roll attractor.

see that gradients of order only a few percent are needed for observable effects. Because the potential energy is subdominant at the initial time, this is only a very small gradient in the initial energy density. Therefore, an initial slice with constant $\dot{\phi}$ is the better choice since we want to work with a FRW metric that requires a homogeneous and isotropic energy density.

If the inflaton field is not uniform, the Klein-Gordon equation, Eq. (1), contains an additional term proportional to $\nabla^2 \phi$. For a gradient in the field, $\phi(x) = A + Bx$ where A and B are constants, $\nabla^2 \phi = 0$ so that we can neglect this term and still work with Eq. (1). The gradient however contributes a term to the energy density of the form $(\nabla \phi)^2/2$, which for a linear gradient in the field ϕ amounts to a constant throughout space. There is also an anisotropic contribution to the pressure proportional to $(\nabla_i \phi)^2$. However, the gradient's contribution to the energy density and pressure is always subdominant for the small amounts of gradients we require so that we can neglect it. Thus, even in the presence of a small spatial gradient, the inflaton field evolves independently at each spatial position. That is, in our approximation the trajectories displayed in Fig. 1 are not modified by the presence of a spatial gradient.

In our extension with a gradient in the initial conditions, two points on opposite sides of the universe which started with different initial values of ϕ will have undergone different amounts of inflation so that the large scale suppression features in the power spectrum associated to an initial fast-roll stage will appear at different scales today. A gradient in e-folds of inflation is the leading effect in our model stretching both the cutoff scale and space by a different amount in different parts of the universe. Certainly, it is not strictly correct to use a FRW background metric and the standard formulas for a uniform and isotropic cosmology. However, the expansion is uniform and isotropic both during the fast roll phase when the kinetic energy is dominant, and later during the slow roll phase. The inhomogeneity only

4

effects the universe during the very short transition region between fast-roll and slow-roll of the inflaton. We feel that our treatment captures the leading effects of an initial gradient without the need to solve exactly the evolution through the short transition region.

3 CMB fluctuations at low multipoles

An initial regime of kinetic energy dominance of the inflaton before reaching the slow-roll attractor modifies the spectrum of quantum fluctuations as noted by CPKL. For wavelengths much smaller than the Hubble scale at the onset of the accelerated expansion, H_*^{-1}, the spectrum is the same as the slow-roll spectrum because the small wavelength perturbations are insensitive to the overall background expansion of the Universe at this time. However, for wavelengths comparable to H_*^{-1} the spectrum is altered and it exhibits a suppression of power for larger wavelengths. Intuitively, this suppression can be understood from the relation $\delta\rho/\rho \sim H^2/\dot{\phi}$: if the inflaton rolls faster initially, the spectrum will be suppressed at larger scales.

Following CPKL, we use a chaotic inflation model with potential $V(\phi) = \frac{1}{2}m^2\phi^2$ with $m = 4 \times 10^{-7}$. As initial conditions, we choose $\phi_i = 3.59$ and $\dot{\phi}_i = -35.9\,m$. This particular choice of initial conditions gives us about 60 e-folds of inflation. The initial kinetic energy is 100 times larger than the initial potential energy so that we start out well in the kinetic energy domination regime.

We use the gauge invariant formalism for cosmological perturbations [22, 23] and the equations of motion for the perturbation variables read

$$\delta\phi_k^{''} + 2\mathcal{H}\delta\phi_k^{'} + \left(\frac{k}{a}\right)^2 \delta\phi_k + V_{,\phi\phi}a^2\delta\phi_k \;=\; 4\phi_0^{'}\Phi_k^{'} - 2V_{,\phi}a^2\Phi_k \tag{5}$$

$$4\pi\phi_0^{'}\delta\phi_k \;=\; \Phi_k^{'} + \mathcal{H}\Phi_k \tag{6}$$

where primes denote differentiation with respect to conformal time η and $\mathcal{H} \equiv a^{'}/a$. We solve these perturbation equations using numerical mode by mode integration. As the system is initially in the kinetic energy domination regime, the vacuum is chosen to be the approximate solution in the kinetic energy domination stage at an initial time η_i [1]

$$v_k(\eta_i) = \sqrt{\frac{\pi}{8\,\mathcal{H}_i}} \; \sqrt{1 + 2\mathcal{H}_i\eta_i} \; H_0^{(2)}\left(k\eta_i + \frac{k}{2\mathcal{H}_i}\right), \tag{7}$$

where the Mukhanov-Sasaki variable is

$$v_k \equiv a\left(\delta\phi_k + \frac{\phi^{'}}{\mathcal{H}}\Phi_k\right). \tag{8}$$

We verified that a different choice of vacuum, the Hamiltonian diagonalization vacuum given by [22]

$$v_k(\eta_i) = \left(k^2 - \frac{z^{''}}{z}\right)^{-1/4}, \quad v_k^{'}(\eta_i) = i\left(k^2 - \frac{z^{''}}{z}\right)^{1/4} \qquad \text{with } z \equiv \frac{a\phi^{'}}{\mathcal{H}} \tag{9}$$

does not change the resulting power spectrum significantly.

In Fig. 2 we show the power spectrum of the gravitational potential after the end of inflation. The cutoff of the spectrum around $k \sim a_0 H_0$ is the most important feature of the spectrum, but some oscillations at the transition to a pure slow-roll spectrum are visible
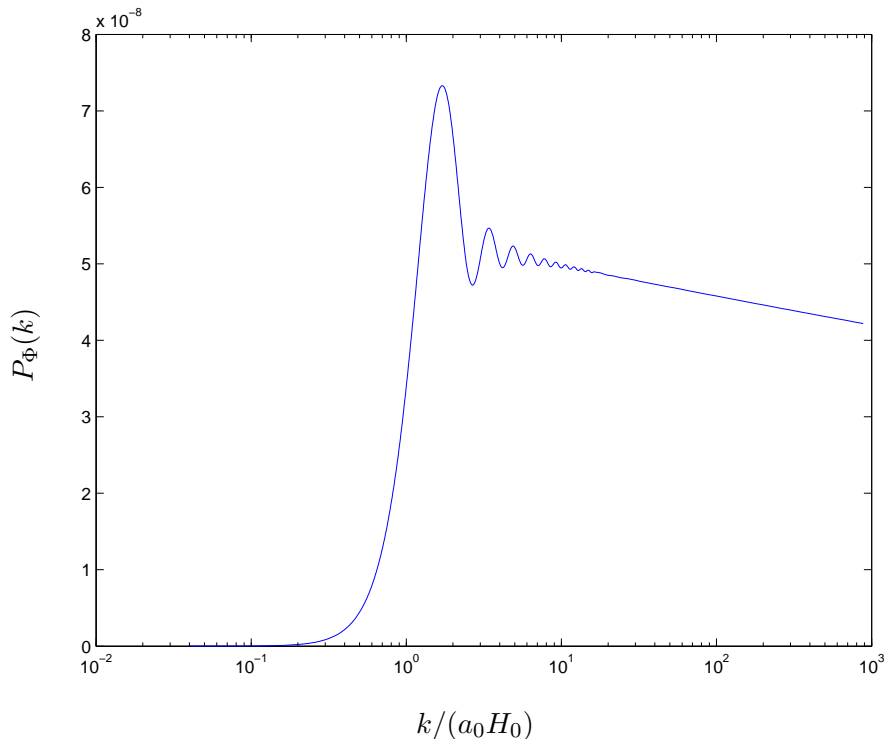
Figure 2: Power spectrum of the gravitational potential Φ at the end of inflation in the CPKL model with an initial fast-roll stage.

as well. The position of the cutoff in the spectrum, *i.e.* the scale associated to the cutoff, actually depends on the complete expansion history of the universe since the onset of inflation until today, which is not exactly known.

Instead of computing the spectrum numerically CPKL have also shown that an approximate analytic solution with an instantaneous transition between the regimes of kinetic energy domination and slow-roll inflation reproduces the exact spectrum extremely well. This shows that the spectrum does not depend much on the details of the inflaton potential. We have checked this by generating the corresponding spectra using ϕ^4 and ϕ^6 potentials, and we found shapes of the resulting power spectra similar to the one shown in Fig. 2 with only small changes in the width of the cutoff region of the order of 10%.

Since the main feature of the spectrum is the cutoff that yields suppression for largest scales, CPKL have also introduced a simple parametrization of a spectrum with an exponential cutoff

$$P_\Phi(k) \sim k^3 |\Phi_k|^2 = A_s \Big(1 - \exp\big[-(k/k_c)^\alpha \big] \Big) k^{n_s - 1} \qquad (10)$$

with $\alpha = 3.35$ as a useful simplified model.

The spectrum of CMB fluctuations can be computed from the primordial power spectrum $P_\Phi(k)$. A variety of astrophysical processes make this a complicated and highly numerical task which is usually performed with numerical codes [24, 25, 26]. Since the power spectrum in wavenumber is not modified at large k, the CMB spectrum will be the same as the standard slow-roll predictions at high multipoles ℓ. At low ℓ the leading effects are the Sachs Wolfe effect and the late time integrated Sachs Wolfe effect. For the calculation of the CMB spectrum we have modified the numerical code CAMB [26] to include the CPKL primordial power spectrum as the initial spectrum. The resulting CMB spectrum is shown in Fig. 3.
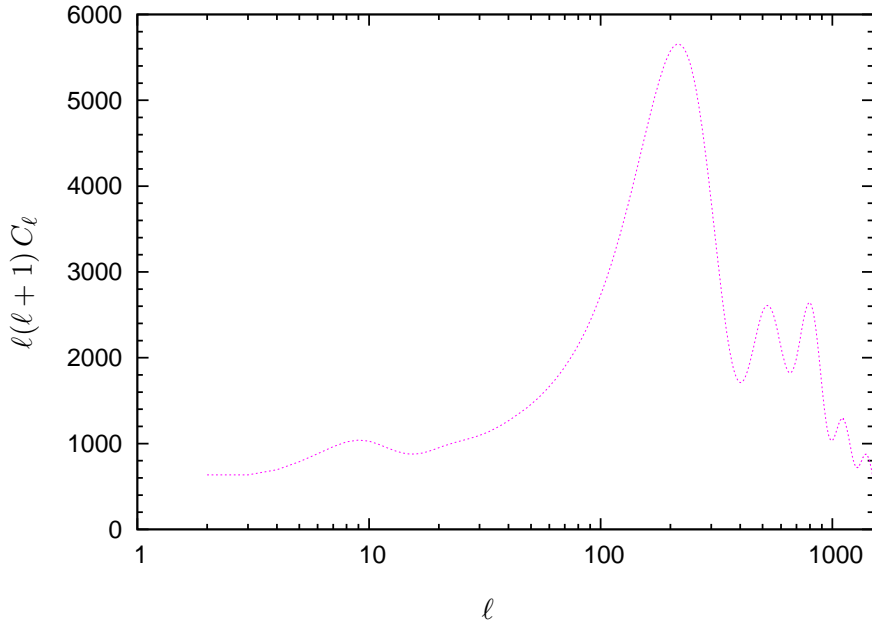
Figure 3: TT power spectrum of the CMB in the CPKL model.

One of the main results is the fact that the features in the primordial spectrum get somewhat smoothed in the CMB spectrum but the shape is generally not altered very significantly. We see the power suppression at low multipoles due to the initial fast-roll stage of the inflaton field, and at high multipoles the spectrum matches the flat slow-roll spectrum. The effect of the wiggles around the cutoff is also evident in the CMB spectrum. However, we note that unlike the primordial spectrum of Fig. 2, the CMB spectrum for multipoles smaller than the scale of the cutoff does not approach zero as quickly, but seems to have an offset which depends on the scale of the cutoff, see also Fig. 4. This offset arises due to the late time integrated Sachs-Wolfe effect which gives contributions to C_ℓ from a wider range of scales than the Sachs-Wolfe effect does. In the presence of a cutoff in the spectrum at large scales, the late time integrated Sachs-Wolfe effect is therefore more important than the Sachs-Wolfe effect at very low ℓ [27].

Since the details of inflation and reheating are not pinned down precisely, the expansion history of the universe is not known exactly and the number of e-folds N during inflation enters as an adjustable parameter, where a minimum of about 60 is needed to solve the flatness and horizon problems. Changing N in our case will shift the position of the feature in the spectrum. For $N \gg 60$, the feature is at scales much larger than our present horizon and the observable CMB spectrum is indistinguishable from a slow-roll spectrum. If two different parts of the universe underwent different amounts of inflation N after the initial fast-roll stage due to different initial conditions ϕ_i and $\dot{\phi}_i$, their spectra will match at small scales or large ℓ as seen in Fig. 4. The power spectrum in the part of the universe that inflated more e-folds will have the scale associated to the feature in the spectrum stretched more so that the feature appears at smaller multipoles ℓ. There is in addition a geometric effect due to a temporary asymmetric expansion, which we explore in the next section. The CPKL mechanism is reasonably predictive in that there is only one free parameter, the scale of the feature in the spectrum, which is determined by the number of e-folds N of inflation and thus by the relative values of the initial conditions for ϕ and $\dot{\phi}$ – see Fig. 1 and Eq. (4). Observationally, this is manifest as the value of ℓ below which there is a suppression in the
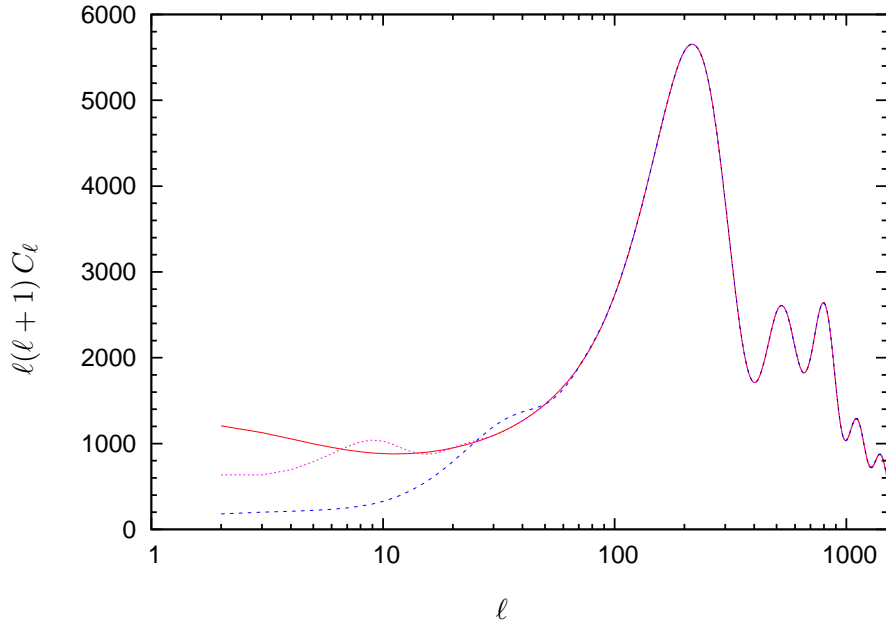
7

Figure 4: CMB spectra for different numbers of e-folds of inflation. The solid line comes from $N \gg 60$ so that the cutoff feature due to an initial fast-roll stage is stretched beyond our observable universe and thus it corresponds to a pure slow-roll spectrum.

CMB power spectrum.

4   Gradient phenomenology and hemisphere analysis

With a spatial gradient in the initial value of ϕ in the frame where $\dot{\phi}$ is uniform, parts with different initial values undergo different amounts of inflation. Once all portions of the observable universe are in the slow-roll phase, the standard inflationary description holds with CMB fluctuations at these scales and subsequent structure formation being spatially uniform. The effect of the initial gradient only modifies the transition region between kinetic domination and slow-roll. This transition yields the cutoff in the spectrum at the scale k that will be stretched by different factors in different parts of the sky due to the presence of the gradient.

Let us consider two different parts of the universe with slightly different initial field values $\phi_{i,1}$ and $\phi_{i,2} = \phi_{i,1} + \Delta\phi$. This also gives different amounts of inflation in the two parts, N_1 and $N_2 = N_1 + \Delta N$ where the difference in e-folds scales proportionally to $\Delta\phi$

$$\Delta N \sim \Delta\phi. \tag{11}$$

Normalizing the scale factor at the initial time, a different amount of e-folds of inflation gives $a_2/a_1 = e^{\Delta N}$ after inflation so that the relationship between coordinates and wavenumbers in the early universe and physical scales today then depends *exponentially* on the difference in e-folds.

Our first task is to understand how a linear gradient in the scalar field translates to variations in the physical scales on the surface of last scatter. Let the coordinate ζ describe the direction along which the initial value of the inflaton field has a linear gradient in the frame where $\dot{\phi}$ is constant, i.e.

$$\phi_i(\zeta) = A + B\zeta . \tag{12}$$

8

A small patch of the initial volume with thickness $d\zeta$ will inflate to a patch of the sky today with a thickness dz in physical coordinates, where z measures distance along the same direction today. Because different patches will have different amounts of inflation, with $a_2/a_1 = e^{\Delta N}$ and $\Delta N \sim \Delta\phi$, the thicknesses will be related by

$$dz = \rho e^{b\zeta} d\zeta. \tag{13}$$

Here ρ is the rescaling of coordinates due to expansion that would have happened without the gradient in the scalar field (with $\phi_i = \phi_i(\zeta = 0) = A$): $\rho \sim a(t_0)/a(t_i)$. The parameter b depends on the magnitude of the gradient $\frac{\Delta\phi}{\Delta\zeta}$ in the inflaton field, with $b = 0$ if there is no gradient in the field. Eq. (13) shows the geometric effect of the gradient on the expansion of space: An initial patch located at a higher ϕ_i than a second patch and separated by a distance $\Delta\zeta$ will inflate $\Delta N = b\Delta\zeta$ e-folds more than the second one, so that the first patch will today be larger in the z-direction by an exponential factor of $e^{\Delta N}$.

The relation in Eq. (13) can be integrated to relate the initial coordinates along the gradient to coordinates today,

$$z = \frac{\rho}{b}(e^{b\zeta} - 1) \tag{14}$$

or

$$b\zeta = \ln\left[1 + \frac{bz}{\rho}\right] \equiv \ln[1 + b'z]. \tag{15}$$

Correspondingly we can relate a feature in the initial wavenumber spectrum, for example the location of the start of the cutoff in wavenumber, to the physical scales today. A cutoff that appears at k_c in the original spectrum would appear at scales

$$k = \frac{k_c}{\rho e^{b\zeta}} \equiv k_0 e^{-b\zeta} \tag{16}$$

today. Rewriting this in terms of the present physical coordinates implies that the feature appears at

$$k = \frac{k_0}{1 + b'z}. \tag{17}$$

It is apparent that due to the geometric effect of different amounts of expansion of different parts of the universe an initial gradient does not yield a simple gradient today! Finally, since we are interested in the CMB radiation coming from the surface of last scatter, we are interested in how this feature varies with direction. If the surface of last scatter is a distance R_* away, and we use $z = R_* \cos\theta$ and define $a = b'R_*$, we have the break in the spectrum occurring at

$$k = \frac{k_0}{1 + a\cos\theta}. \tag{18}$$

The result is that an initial gradient in the scalar field, or equivalently in the start of the slow-roll phase, leads to the break in the CMB power spectrum occurring at a wavenumber that depends on the position in the sky by the above relation.

It is tempting to translate Eq. (18) into a relation for the cutoff position in terms of angles or multipoles in the CMB spectrum and use it to find the CMB modulation function for this model with a gradient. This is quite easy to do using the approximate primordial CPKL spectrum from Eq. (10) and only taking into account the Sachs-Wolfe effect which results in a C_ℓ spectrum of the same form as Eq. (10) (see the second toy model analysis in the Appendix). However as we have pointed out in the last section, the late time integrated Sachs-Wolfe effect is important at low ℓ, and its inclusion unfortunately does not seem to result in a simple analytic modulation function.
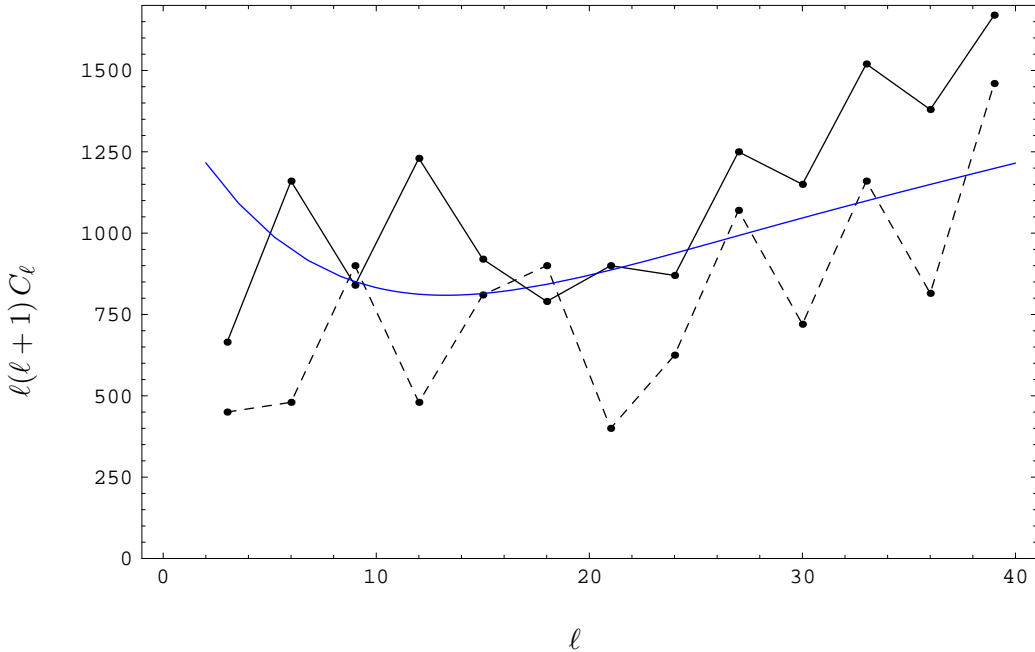
Figure 5: Sketch of the measured CMB power spectra (mimicking the right panel of Fig. 7 in Ref. [12]) for the northern hemisphere (connected by dashed lines) and for the southern hemisphere (connected by solid lines), and the WMAP-3 best fit ΛCDM spectrum C_ℓ^0 (smooth blue curve) [28].

A more rigorous test of the model would be to calculate the general correlations $\left\langle a_{\ell'm'}^* a_{\ell m} \right\rangle$ including off-diagonal terms which vanish in the homogeneous and isotropic limit and compare these correlations to CMB data, as proposed for a different anisotropic model in [17]. Such an analysis would go beyond the scope of this paper. Instead we will perform a simple first test of our model making use of the existing data in which the CMB power spectrum is extracted separately from two hemispheres of the sky.

Data in hemisphere form has been reported by [5, 11, 12] and we sketch the results of the analysis of the WMAP 3-year data of [12] in Fig. 5. The two measured CMB spectra displayed are extracted from the two hemispheres with respect to the maximum asymmetry axis pointing to the north pole $(\theta, \phi) = (80°, 57°)$ in galactic coordinates, and the power spectrum for $\ell < 40$ obtained from the northern hemisphere exhibits a lack of power compared to the power spectrum of the southern hemisphere.

In order to perform a first test of our model with an initial fast-roll stage and a spatial gradient in the initial field value, we approximate our results by performing a hemisphere averaging of the CMB spectrum and compare our predictions to the measured data in Fig. 5. For that we orient our initial gradient in the direction of the maximum asymmetry axis observed. Furthermore, we identify the point of the gradient with the lowest field value (where we expect the least amount of inflation and thus a cutoff feature in the spectrum present at smaller scales or higher ℓ than the rest of the gradient) as the north pole. That then has the potential to yield a spectrum close to the observed one with a suppression in the northern hemisphere.

Due to the fact that parts of the universe with different initial field values undergo different amounts of inflation, we first have to clarify what initial conditions lead to two equally sized hemispheres today. We start with the northern hemisphere (N) which contains the point with
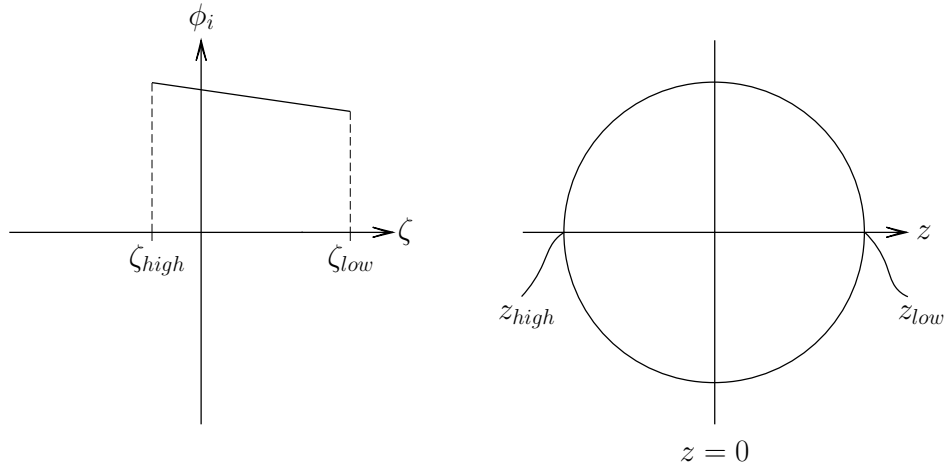
Figure 6: The gradient in ϕ_i shown in the original coordinates ζ which are transformed into coordinates z in the present universe in which the surface of last scattering is shown.

the lowest initial field value of the gradient, *i.e.* the lower part of the gradient, and choose a certain amount of initial gradient to give the northern hemisphere today. This setup is sketched in Fig. 6 in the coordinate ζ and in today's physical coordinate z which are aligned with the gradient and the maximum asymmetry axis, and we normalize the coordinates such that the point $\zeta = 0$ becomes $z = 0$ today. If at $\zeta = 0$ we expect $N = N_0$ e-folds, at the north pole, *i.e.* the lowest point of the gradient $\zeta = \zeta_{low}$, the amount of inflation is $N = N_0 - \Delta N_{low}$. Since the number of e-folds scales linearly with the initial field value, the number of e-folds as a function of the spatial coordinate ζ is

$$N(\zeta) = N_0 - \Delta N_{low} \frac{\zeta}{\zeta_{low}}. \tag{19}$$

Now we are interested in the size of this hemisphere today which follows from integrating $dz = e^{\mathcal{N}} e^{N(\zeta)} d\zeta$ where $\mathcal{N}$ is the number of e-folds of the expansion of the universe since the end of inflation:

$$z_{low} = e^{\mathcal{N}} e^{N_0} \zeta_{low} \frac{1 - e^{-\Delta N_{low}}}{\Delta N_{low}} \tag{20}$$

which gives us the radius of the first hemisphere, i.e. the part of the gradient that inflated the least. As we want to construct two hemispheres of equal size, we require the size of the southern hemisphere (S) which contains the highest part of the gradient to be equal to the size of the northern hemisphere,

$$z_{high} = -z_{low}. \tag{21}$$

With the relation between the coordinates ζ and z, we can in turn determine

$$\zeta_{high} = -\zeta_{low} \frac{\log 2 - e^{-\Delta N_{low}}}{\Delta N_{low}} \tag{22}$$

and find the number of e-folds for the point with most inflation from Eq. (19) to be

$$N(\zeta_{high}) = N_0 + \log\left(2 - e^{-\Delta N_{low}}\right). \tag{23}$$

This result is interesting because it means that no matter how large a gradient there is in the northern hemisphere, the gradient in the southern hemisphere will at most give a difference

11

of $\log 2 \approx 0.69$ e-folds of inflation within the southern hemisphere. This illustrates that parts of the universe with lower initial field values expand exponentially less than parts with higher field values so that the parts with highest initial field values dominate the universe today and parts with lowest initial field values comprise only a tiny fraction of the universe.

For a power spectrum with a feature that varies as a function of position ζ or z, we have to average the power spectrum over the two hemispheres in order to compare with the measured spectrum sketched in Fig.5. Our approximation to this averaging is to imagine to cut each hemisphere into slices. If we use slices of equal thickness Δz in today's coordinates, we take the average over all slices of the hemisphere by weighing each slice by its number of measured points on the surface of last scattering. The number of measured points is assumed to be proportional to the surface area of a slice, and since the surface area of a spherical segment only depends on its thickness Δz and the radius of the sphere, each slice of equal thickness has the same weight in the average over the hemisphere.

In the Appendix we present a simple toy model with a step function cutoff as the primordial fluctuation spectrum. It is illustrative since most parts of the calculation can be performed analytically. Our analysis here however is performed completely numerically. We approximate our gradient by a series of equidistant steps and calculate the C_ℓ spectra for each of the steps with a constant ϕ_i, *i.e.* we use equidistant (in coordinate ζ) slices of the gradient in which we approximate the initial field as constant. When averaging over a hemisphere, we have to average over all steps contained in the hemisphere. The geometric effect of different amounts of expansion of the different slices is accounted for by the weight factor $\exp\left(-\Delta N_{low} \frac{\zeta}{\zeta_{low}}\right)$ for each step, where we take the position ζ of the slice as its center value. The effect of our mechanism on the averaged CMB spectra of the two hemispheres is best illustrated by defining relative suppression functions

$$F_\ell^D = C_\ell^D / C_\ell^{SR} \tag{24}$$

with $D = N, S$ as the ratio of the CMB spectra for the two hemispheres and the CAMB spectrum we obtain for pure slow-roll inflation.

The two free parameters then in this hemisphere averaging procedure are the initial field values $\phi_i(\zeta = 0)$ and $\phi_i(\zeta = \zeta_{low})$, which then determine $\phi_i(\zeta = \zeta_{high})$ as well as N_0, ΔN_{low} and ΔN_{high}. In order to find a good fit to the hemisphere data in Fig. 5, we first generate a large array of slice spectra using CAMB. Here, we use slices which have a thickness $\Delta\zeta$ corresponding to $\Delta N_{slice} = 0.1$, *i.e.* the difference in number of e-folds between two adjacent slices is 0.1. In order to achieve the best fit to the data points for the two hemispheres, we vary the number of slices for the hemispheres (mostly the number of slices for the northern hemisphere since $\Delta N_{high} \approx 0.7$ for almost all of parameter space) and we vary the location of the border between the two hemispheres within our array of slices. That then corresponds to varying $\phi_i(\zeta = 0)$ and $\phi_i(\zeta = \zeta_{low})$. For each possibility, we obtain the suppression functions F_ℓ^N and F_ℓ^S for both hemispheres. These are then multiplied by the best fit ΛCDM curve C_ℓ^0 for the WMAP 3-year data (see the smooth curve in Fig. 5) to yield our mechanism's prediction for each hemisphere

$$C_\ell^{Theory, D} = F_\ell^D C_\ell^0 \tag{25}$$

with $D = N, S$. Here, $C_\ell^{Theory, D} = C_\ell^D$ if all parameters in CAMB are selected exactly as for the WMAP 3-year best fit. Since we use the slow-roll inflation spectrum in CAMB to obtain C_ℓ^{SR} instead of a parameterized spectrum with a different spectral index, there could be small deviations due to the normalization of the CMB spectra, and we correct for these by using Eq. (25). The optimal configuration is then found from a χ^2 fit to the data points
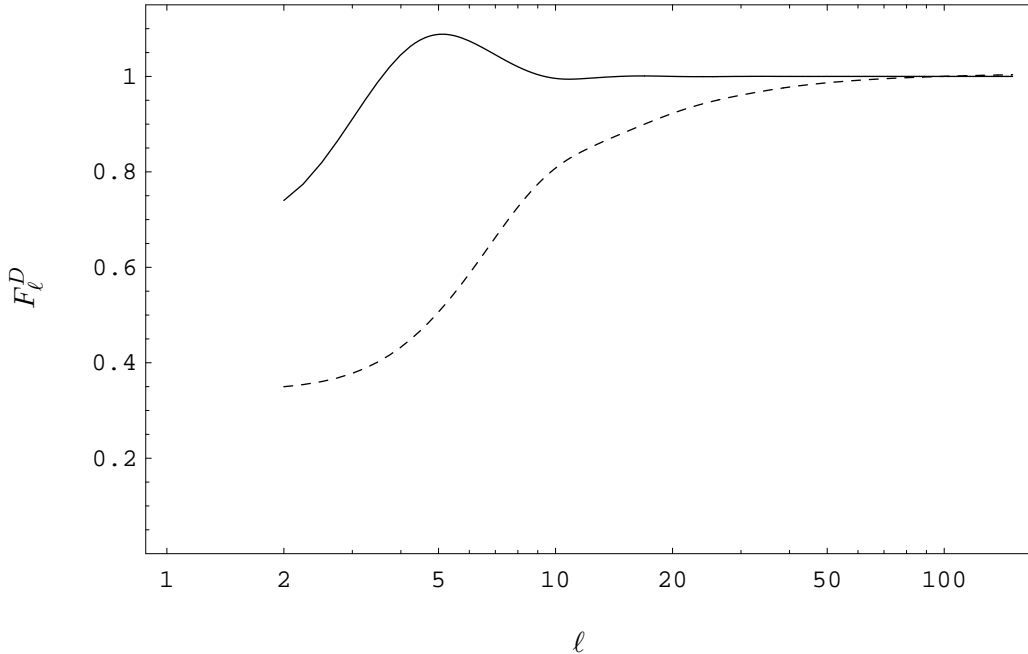
Figure 7: Suppression functions resulting from averaged CPKL spectra for the northern (dashed) and southern (solid) hemisphere for $\Delta N_{low} = 3.6$.

in Fig. 5 calculating

$$\chi^2 = \sum_{D=N,S} \sum_{\ell} \frac{\left(C_\ell^{Theory,D} - C_\ell^{Data,D}\right)^2}{\left(\sigma_\ell^D\right)^2}, \tag{26}$$

where the variance is taken as the cosmic variance of the theoretical spectrum of the hemisphere, $\sigma_\ell^D = \sqrt{2/(2\ell+1)}\, C_\ell^{Theory,D}$.

The best-fit configuration has $\Delta N_{low} = 3.6$ and $\Delta N_{high} = 0.7$ which corresponds to less than 4% of variation in ϕ_i over both hemispheres together. In Fig. 7 we display the resulting suppression functions F_ℓ^D for both hemispheres. The spectrum of the southern hemisphere for the best fit is close to a slow-roll spectrum with little suppression only at very largest scales. For the northern hemisphere, the spectrum shows a suppression which is most significant at $\ell < 10$. Due to the large range of e-folds $\Delta N_{low} = 3.6$, the averaged spectrum of the northern hemisphere does not exhibit any peak because the peaks of the individual spectra of the slices average out.

When compared to the uniform and isotropic ΛCDM slow-roll CMB spectrum, we find that χ^2 decreases, $i.e.$ improves, by 3.1 for our model in the optimal configuration. Moreover, the prediction for the quadrupole $\ell = 2$ for the full sky sphere is reduced by 45% in our model compared to the ΛCDM best fit prediction. However, this does not indicate that a significant preference for our fast-roll with gradient model arises: even though the decrease of $\Delta\chi^2 = -3.1$ improves the χ^2, the model introduces four new parameters when compared to the ΛCDM model – two angles for the direction of the gradient, the amount of gradient used ΔN_{low} and a scale k_0 at which the cutoff appears in a uniform spectrum of one of the slices.

As one can see from Fig. 7, a significant suppression only arises for the lowest mutipoles $\ell \lesssim 10 - 20$. The reason for that is the geometric effect of the gradient which causes the

13

regions of the gradient with higher initial field values to dominate the universe, so that the resulting averaged hemisphere spectra still exhibit relatively steep cutoffs which are relatively close to each other. For the suppression functions of the hemispheres for the best fit shown in Fig. 7 the cutoff in the northern hemisphere's spectrum is roughly at $\ell \sim 2$ whereas for the southern hemisphere it is at $\ell \sim 7$. That makes it hard to improve the χ^2 more significantly, since the hemisphere data sketched in Fig. 5 can be roughly characterized as a constant suppression of order 20% up to $\ell \sim 40$. Moreover, the errors dominated by cosmic variance are reduced for suppressed theoretical spectra so that scattered data points can easily spoil the χ^2.

In the Appendix we additionally discuss two toy models. The first one uses a step-function primordial spectrum, which allows us to perform parts of the hemisphere averaging analytically without having to approximate the gradient as steps. As a second toy model we consider a primordial spectrum of the same form as Eq. (10) but with a significantly softer cutoff than the CKLP spectrum. Such a more gradual cutoff could potentially achieve an asymmetry reaching to higher values of ℓ.

5   Conclusions

The data appears to suggest a spatial modulation in the CMB power spectrum. However, this asymmetry is unusual in that it may only be present at largest scales or multipoles $\ell \lesssim 40$. If inflation lasts only about 60 e-folds, this can occur if at the earliest stages of inflation there is an asymmetry which however disappears at later times of inflation. Provided the later stages of inflation are governed by a single slowly rolling field, the power spectrum at high ℓ and the universe today will be homogeneous and isotropic. However the quantum fluctuations at the earliest times, and hence the power spectrum at low multipoles, will show evidence of the initial lack of isotropy.

We have provided a model of how this situation could have developed within the framework of single field inflation. It is based on the CPKL mechanism for large scale power suppression due to an initial fast-roll stage paired with a gradient in the initial values of the inflaton field. A gradient in the initial conditions is manifest as differing numbers of e-foldings of slow-roll behavior on different sides of the universe. This amounts to shifts in the ℓ values at which the suppression of the CMB power at large angular scales occurs. This model has a distinctive pattern for the generation of spatial asymmetries which makes it very predictive, and apart from the asymmetry axis, there are only two additional parameters characterizing the position of the cutoff and the amount of gradient within the observable universe.

Our simple analysis where we approximated the initial gradient by a series of steps and averaged these over two hemispheres provided a first comparison to WMAP data extracted from different hemispheres. While our model reproduces the qualitative features of the data and improves the fit by $\Delta\chi^2 = -3.1$, we cannot claim a preference for our model since it involves the introduction of in total four new parameters. Because of the geometric effect on the expansion of space resulting from differing amounts of inflation due to the initial gradient, a much better fit in a hemisphere analysis is hard to achieve with our simple single field model with an initial fast-roll stage and a gradient. Nevertheless, one could improve on our analysis by performing a full covariance analysis of the model including all anisotropic degrees of freedom, such as studied in [17]. In this way, one would use the information contained in the general correlations $\langle a_{\ell'm'}^* a_{\ell m} \rangle$, including off-diagonal terms which vanish in the homogeneous and isotropic limit.

It is also possible to generate spatial asymmetries in the power spectrum through the use of two or more fields. In this case, it is possible to assume that one field has a spatial gradient

in the frame in which the other field is uniform. Here there is a lot more freedom. With two fields, each field has its own potential with the possibility of a cross coupling between the fields. These possibilities enable one to modify the shape of the inflaton potential in different ways either enhancing or suppressing the rolling of the inflaton field and also modifying the amount of quantum fluctuations. The resulting possibilities for generating asymmetries deserve further study. Such models are more flexible, but are inherently less predictive than the single field model studied in this paper. However, at least some of these theories could have a similar phenomenology. By providing an initial faster evolution, one can suppress the curvature fluctuations providing a cutoff in the fluctuation spectrum, and a gradient in this initial condition would survive for only a few e-foldings. With the additional freedom in multi field models, one may be able to find a model where the geometric effect which limits our single field model's capability to obtain a significant asymmetry between hemispheres extending beyond $\ell \sim 10 - 20$ is absent or less restrictive.

We note also that our model, and possible generalizations, have the potential to impact the analyses of other anomalies. For example, the cold spot uncovered in [8] occurs along the same axis as the power spectrum modulation. In our model the primary effect is the lack of power in some direction. Our hemisphere fit suggested that one hemisphere is close to the pure slow-roll while the other hemisphere shows the suppression. This could be similar in effect to the existence of a cold spot. Likewise, it is possible that this mechanism can modify the analysis of the unusual quadrupole-octopole alignments. When attempting a partial wave decomposition, an overall dipole shifts the underlying power from one multipole to neighboring ones with $\Delta\ell = \pm 1$. Our modulation in the spectrum is not exactly a dipole, but could nevertheless shift the apparent power from one multipole to nearby ones.

It would be interesting to see if the addition of this form of spatial gradient to the studies that fit the CMB spectrum can provide further understanding of the proposed anomalies that are discussed in the literature. For that a more involved comparison to data than ours is needed. If the mechanism was successful it would add to our understanding of inflation and would increase the confidence in the inflationary paradigm.

Appendix

In the Appendix, we study two toy models. The one considered first with a step function cutoff spectrum is instructive since the hemisphere averaging for the primordial power spectrum can be obtained analytically. For the second toy model we use an exponential cutoff spectrum which falls off more gradually than the CPKL spectrum.

We construct the theta function toy model keeping the main aspects of the gradient fast-roll model, a large scale cutoff in the power spectrum whose scale varies within the universe due to a gradient in the number of e-folds of inflation. Thus, the scale of the cutoff in the spectrum varies spatially according to Eq. (16), but we will approximate the spectrum of the
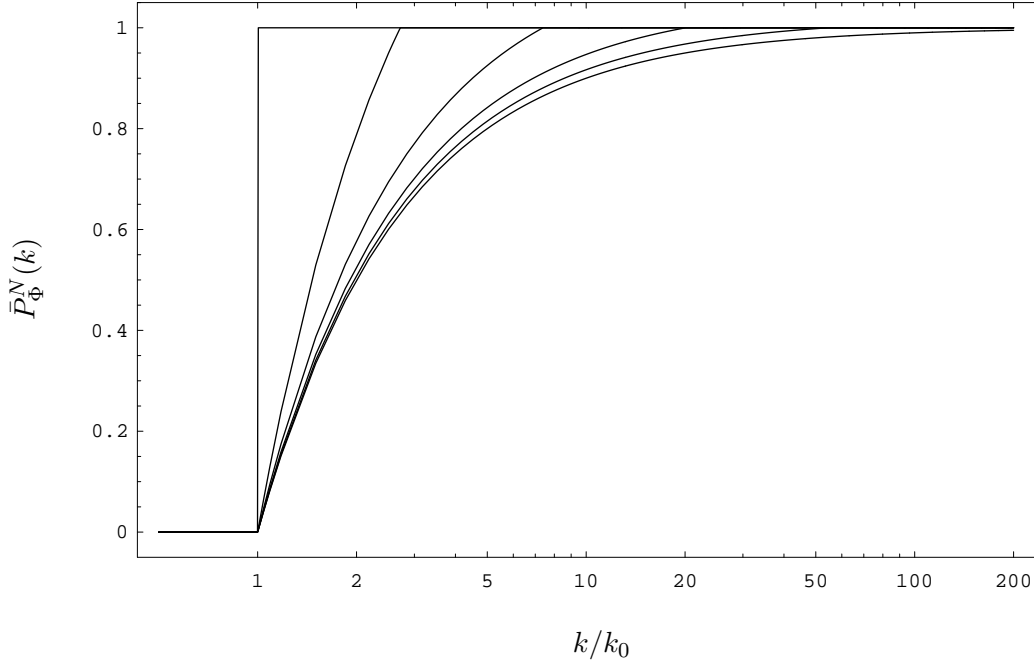
Figure 8: Averaged theta function spectra for the northern hemisphere for differing amounts of gradients such that $\Delta N_{low} = 0, 1, 2, 3, 4, \infty$.

uniform fast-roll model of Fig. 2 by a simple theta function cutoff spectrum $P_\Phi(k) = \Theta(k-k_c)$. For simplicity, we do not include a spectral index and we compare the resulting spectra to a scale invariant Harrison-Zel'dovich spectrum.

In the hemisphere analysis in Sec. 4 we first calculated CMB spectra and then performed an average over the two hemispheres. Here however, we will first average the primordial spectrum over the hemispheres and then calculate the CMB power spectra. The primordial spectra for the northern and southern hemispheres are

$$\bar{P}_\Phi^N(k) = \int_0^{z_{low}} dz\, P_\Phi(k, z) = \int_0^{\zeta_{low}} d\zeta \, \exp\left(-\Delta N_{low} \frac{\zeta}{\zeta_{low}}\right) P_\Phi(k, \zeta)$$

$$\bar{P}_\Phi^S(k) = \int_{z_{high}}^0 dz\, P_\Phi(k, z) = \int_{\zeta_{high}}^0 d\zeta \, \exp\left(-\Delta N_{low} \frac{\zeta}{\zeta_{low}}\right) P_\Phi(k, \zeta) \qquad (27)$$

from which we can calculate the averaged CMB spectra C_ℓ^N and C_ℓ^S. As seen in Eq. (16) today's physical scale of the cutoff in the spectrum varies exponentially such that the spectrum becomes

$$P_\Phi(k, \zeta) = \Theta\left[k - k_0 \exp\left(+\Delta N_{low} \frac{\zeta}{\zeta_{low}}\right)\right] \qquad (28)$$

where the position of the cutoff in the northern hemisphere varies from k_0 to $k_{low} = k_0 e^{\Delta N_{low}}$ depending on the position ζ. Plugging this into Eq. (27) we obtain an average spectrum

$$\bar{P}_\Phi^N(k) = \frac{1 - k_0/k}{1 - k_0/k_{low}} \, \Theta(k - k_0) \, \Theta(k_{low} - k) + \Theta(k - k_{low}) \qquad (29)$$

for the northern hemisphere which vanishes for $k < k_0$ and equals unity for $k > k_{low}$.
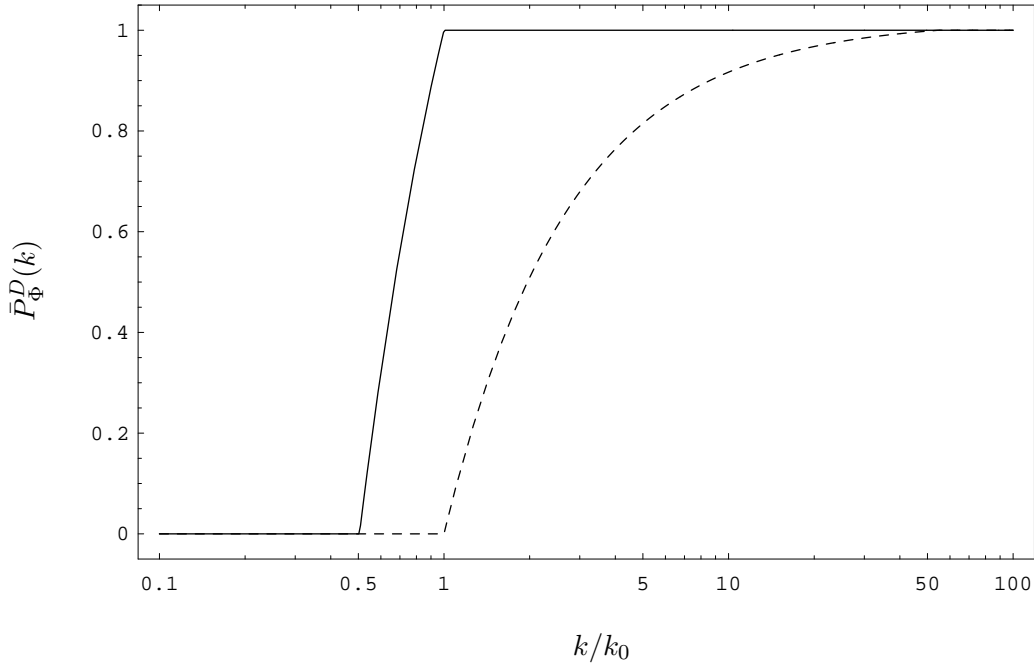
16

Figure 9: Averaged theta function spectra for the northern (dashed) and southern (solid) hemisphere for $\Delta N_{low} = 4$.

In Fig. 8 we display the averaged spectrum of the northern hemisphere for different amounts of gradient, *i.e.* for different ΔN_{low}, where the limit $\Delta N_{low} = 0$ corresponds to no gradient at all and we recover a pure theta function spectrum, whereas the limit $\Delta N_{low} = \infty$ corresponds an infinite amount of gradient within the hemisphere. As one would expect, the average spectrum of the hemisphere is dominated by the part of the gradient with most e-folds of inflation which will dominate and make the average power spectrum rather steep around k_0. At $k/k_0 = 10$ the spectrum already reaches 0.9 in the limit of an infinite gradient, and since $\ell \sim k$ in the CMB spectrum, we expect that the cutoff in the resulting averaged C_ℓ spectrum is also rather steep with a range of significant suppression up to roughly $\ell \sim 10$.

The averaged spectrum for the southern hemisphere can be calculated analogously, and for $\Delta N_{low} = 4$, we show both averaged spectra in Fig. 9. The averaged spectrum of the southern hemisphere is steeper than the spectrum of the northern hemisphere since it contains a much smaller piece of the initial gradient with a difference of only about 0.69 e-folds inside the southern hemisphere as compared to $\Delta N_{low} = 4$ e-folds of difference in the northern hemisphere.

As the next step we numerically calculate the CMB spectrum C_ℓ, where for this toy model we will only account for the Sachs Wolfe effect [29] [30]

$$C_\ell = \frac{4\pi}{9} \int_0^\infty \frac{dk}{k} \, j_\ell^2 \left(\frac{2k}{H_0} \right) P_\Phi(k), \tag{30}$$

ignoring all other effects such as the integrated Sachs-Wolfe effect. These Sachs-Wolfe spectra for the northern and the southern hemispheres are divided by the Sachs-Wolfe spectrum of a scale invariant Harrison Zel'dovich spectrum to find the suppression functions F_ℓ^N and F_ℓ^S for both hemispheres. For that we have to specify the scale k_0. We choose $k_0 = a_0 H_0$ such that the CMB spectrum of the northern hemisphere ($z = 0 \dots z_{low}$) will exhibit a suppression of
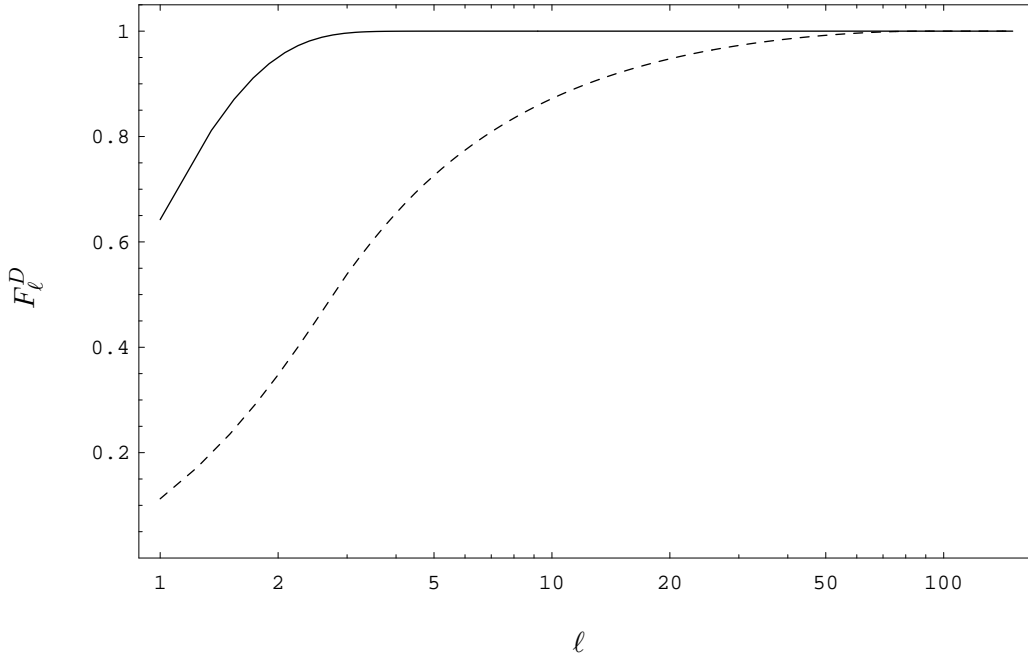
17

Figure 10: Suppression functions resulting from an averaged theta function spectra for the northern (dashed) and southern (solid) hemisphere for $\Delta N_{low} = 4$. Note that the underlying calculation neglected the integrated Sachs-Wolfe effect.

power at largest scales, whereas the CMB spectrum of the southern hemisphere $z = z_{high} \ldots 0$ will exhibit (almost) no large scale suppression. The resulting suppression functions F_ℓ^N and F_ℓ^S are shown in Fig. 10, and as one would expect, their shapes do not differ much from the primordial averaged power spectra in Fig. 9. At small scales or high ℓ, both spectra match onto the CMB spectrum from a scale invariant primordial spectrum, and for observable multipoles $\ell \geq 2$ the southern spectrum doesn't significantly vary from a featureless spectrum. The spectrum of the northern hemisphere however is significantly suppressed at low ℓ, but as expected, for $\ell \gtrsim 12$ the suppression becomes smaller than 10%.

We can test our theta function cutoff toy model by calculating the χ^2 of the measured CMB data points in Fig. 5 with respect to the averaged spectra of the two hemispheres. The resulting χ^2 for the northern hemisphere decreases by 2.6 in comparison to the isotropic ΛCDM model whereas χ^2 doesn't change significantly for the southern hemisphere. Unlike in Sec. 4 where we fitted the parameters and obtained $\Delta\chi^2 = -3.1$ for the best fit, here we simply chose plausible parameters k_0 and ΔN_{low}.

For this toy model, we have only considered the Sachs-Wolfe contributions to the CMB anisotropies, ignoring the integrated Sachs-Wolfe effect etc. Nevertheless, when we compare the hemisphere suppression functions in Figs. 7 and 10, we note that neither the precise form of the cutoff nor the inclusion of the integrated Sachs-Wolfe effect seem to change the main features. At the very lowest multipoles $\ell < 5$ one can see in Fig. 7 the effect of the integrated Sachs-Wolfe effect resulting in a plateau instead of a cutoff extending down to zero. The main features however are determined by the geometric effect due to a gradient in the number of e-folds and by the steepness the cutoff feature in the spectrum.

Before proceeding to study the next toy model, we will briefly comment on the integrated Sachs-Wolfe effect which we omitted in the analysis of the above toy model. As mentioned
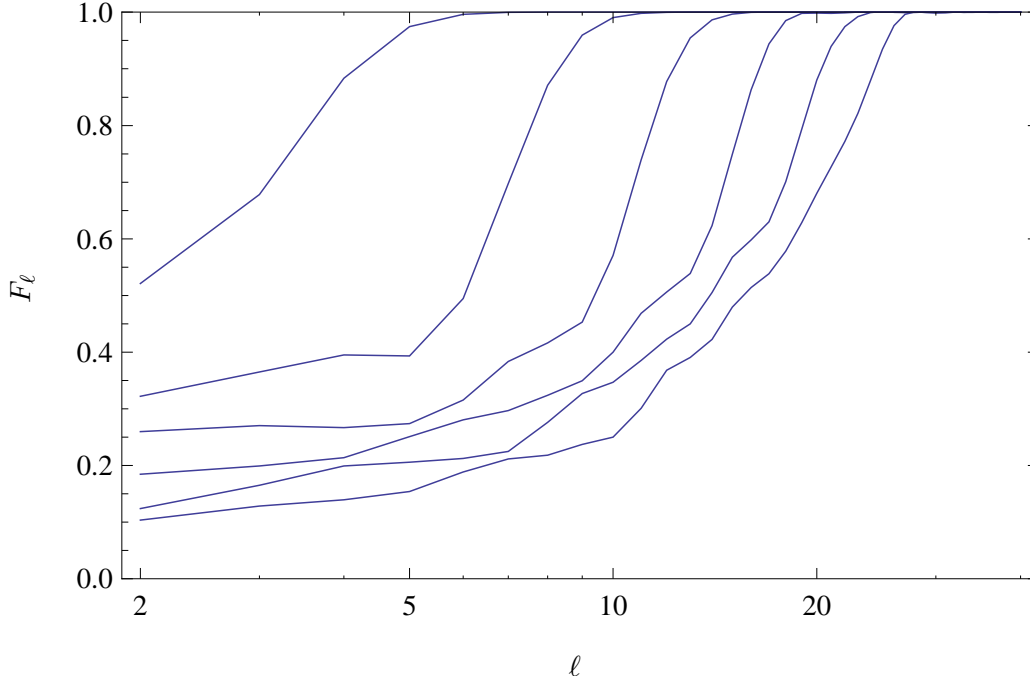
Figure 11: Suppression functions from fully numerical CMB spectra resulting from *uniform* primordial theta function spectra with the cutoff position varied linearly in k. The plateau to the left of each cutoff arises due to the integrated Sachs-Wolfe effect, and its height depends on the location of the cutoff.

earlier, the integrated Sachs-Wolfe effect gives contributions to C_ℓ from a wider range of scales than the Sachs-Wolfe effect does. Therefore at scales larger than the scale associated with the cutoff, the Sachs-Wolfe effect contributes almost nothing to the CMB power spectrum but the integrated Sachs-Wolfe effect can still yield some power in that region. That gives the plateaus or offsets in the CMB spectrum. To illustrate these plateaus, it is most transparent to show the CMB spectrum resulting from a uniform theta function primordial spectrum, as seen in Fig. 11 for various cutoff scales. We observe that the height of the offset depends on the scale of the cutoff where smaller cutoff scales result in a lower offset.

At the other extreme from a step function cutoff is one for which the cutoff can be made gradual. This can be modeled by use of the exponential cutoff spectrum introduced in Eq. (10) where we allow for the exponent α to take on different values. The parameter α governs the steepness of the cutoff in the spectrum. For low values of α we obtain spectra which exhibit a slowly varying cutoff rather than the steep cutoff for $\alpha = 3.35$. This latter value mimics the the CPKL fast-roll spectrum, and larger values than this would approach the step function. Here we explore the softer cutoff provided by small values of α. As we did for the theta function model, we keep the aspect of a gradient in the number of e-folds of inflation. The resulting scenario may be relevant for other models, with the basic features of an IR cutoff of the perturbation spectrum with the scale of the cutoff varying spatially as dictated by a gradient in the number of e-folds of inflation.

As we did in the case of the theta function spectrum analysis, we do not include a spectral
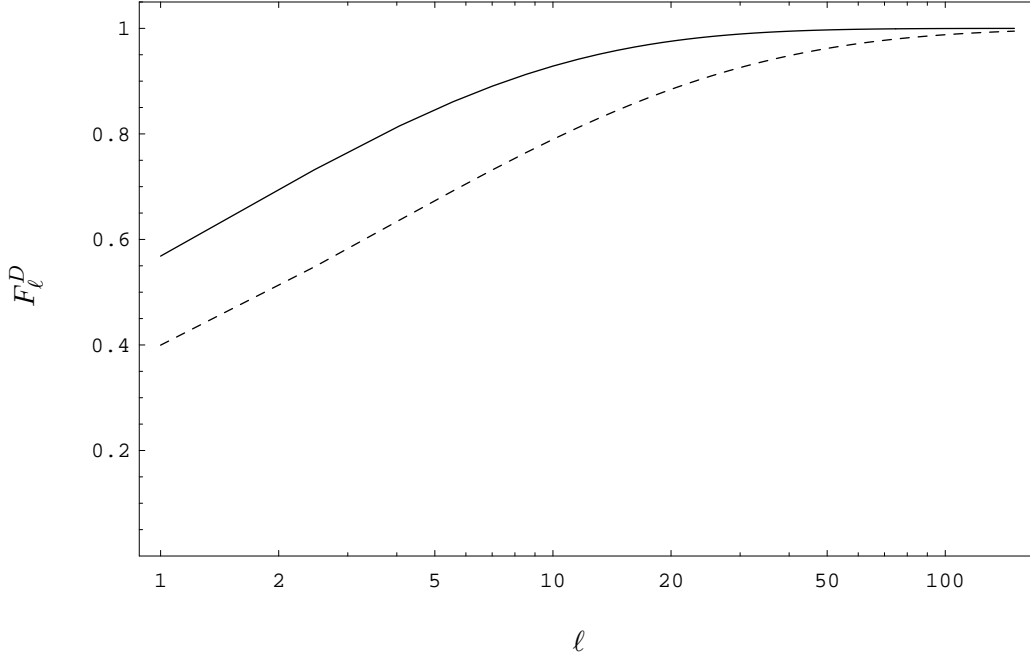
Figure 12: Suppression functions resulting from averaged exponential spectra for the northern (dashed) and southern (solid) hemisphere for $\bar{\alpha} = 0.5$, $\ell_0 = 2$ and $\Delta N_{low} = 2$. Note that the underlying calculation neglected the integrated Sachs-Wolfe effect.

index so that Eq. (10) simplifies to

$$P_\Phi(k) = 1 - \exp\left[-(k/k_c)^\alpha\right]. \tag{31}$$

We find that when one numerically calculates the Sachs-Wolfe spectrum of such an exponential cutoff spectrum via Eq. (30), the resulting Sachs-Wolfe spectrum is approximated extremely well by an exponential cutoff spectrum for $\ell(\ell+1)\,C_\ell$ (where the exponential $\bar{\alpha}$ for the Sachs-Wolfe spectrum is a bit smaller than α in $P_\Phi(k)$). Ignoring again the integrated Sachs-Wolfe effect, we can therefore use

$$\ell(\ell+1)\,C_\ell = 1 - \exp\left[-(\ell/\ell_c)^{\bar{\alpha}}\right] \tag{32}$$

where now the position of the cutoff in ℓ space varies spatially as

$$\ell_c = \ell_0 \exp\left(+\Delta N_{low}\,\frac{\zeta}{\zeta_{low}}\right) \tag{33}$$

so that

$$C_\ell(\zeta) = \frac{1}{\ell(\ell+1)}\left(1 - \exp\left[-\left(\frac{\ell}{\ell_0 \exp\left(+\Delta N_{low}\,\frac{\zeta}{\zeta_{low}}\right)}\right)^{\bar{\alpha}}\right]\right). \tag{34}$$

To find the averaged spectra for the two hemispheres, we integrate over the position dependent spectrum analogously to Eq. (27)

$$C_\ell^N = \int_0^{\zeta_{low}} d\zeta\,\exp\left(-\Delta N_{low}\,\frac{\zeta}{\zeta_{low}}\right)\,C_\ell(\zeta)$$

$$C_\ell^S = \int_{\zeta_{high}}^0 d\zeta\,\exp\left(-\Delta N_{low}\,\frac{\zeta}{\zeta_{low}}\right)\,C_\ell(\zeta). \tag{35}$$

20

For the parameters $\bar{\alpha} = 0.5$, $\ell_0 = 2$ and $\Delta N_{low} = 2$, the suppression functions F_ℓ^D for $D = N, S$ are displayed in Fig. 12. From this we see that it is possible to have a suppression factor that extends out to larger values of ℓ, and which creates an asymmetry on the sky. Treated simply as a suppression of the standard WMAP spectrum, this modification will not lead to an improved fit because the suppression of the power spectrum occurs in both hemispheres. It is possible that a better fit could be obtained if one adjusts the magnitude of the power spectrum, but this would involve adjustments of all the astrophysical parameters in order to not upset the agreement obtained at smaller angular scales.

References

[1] C. R. Contaldi, M. Peloso, L. Kofman and A. Linde, "Suppressing the lower Multipoles in the CMB Anisotropies," JCAP **0307**, 002 (2003) [arXiv:astro-ph/0303636].

[2] A. H. Guth, "The Inflationary Universe: A Possible Solution To The Horizon And Flatness Problems," Phys. Rev. D **23**, 347 (1981).
A. D. Linde, "A New Inflationary Universe Scenario: A Possible Solution Of The Horizon, Flatness, Homogeneity, Isotropy And Primordial Monopole Problems," Phys. Lett. B **108**, 389 (1982).
A. Albrecht and P. J. Steinhardt, "Cosmology For Grand Unified Theories With Radiatively Induced Symmetry Breaking," Phys. Rev. Lett. **48**, 1220 (1982).
For details, see A. D. Linde, *Particle Physics and Inflationary Cosmology*, (Harwood, Chur, Switzerland, 1990) [arXiv:hep-th/0503203].

[3] D. N. Spergel *et al.*, "Wilkinson Microwave Anisotropy Probe (WMAP) three year results: Implications for cosmology," arXiv:astro-ph/0603449.

[4] H. K. Eriksen, F. K. Hansen, A. J. Banday, K. M. Gorski and P. B. Lilje, "Asymmetries in the CMB anisotropy field," Astrophys. J. **605**, 14 (2004) [Erratum-ibid. **609**, 1198 (2004)] [arXiv:astro-ph/0307507].

[5] F. K. Hansen, A. J. Banday and K. M. Gorski, "Testing the cosmological principle of isotropy: local power spectrum estimates of the WMAP data," Mon. Not. Roy. Astron. Soc. **354**, 641 (2004) [arXiv:astro-ph/0404206].

[6] C. G. Park, "Non-Gaussian Signatures in the Temperature Fluctuation Observed by the WMAP," Mon. Not. Roy. Astron. Soc. **349**, 313 (2004) [arXiv:astro-ph/0307469].

H. K. Eriksen, D. I. Novikov, P. B. Lilje, A. J. Banday and K. M. Gorski, "Testing for non-Gaussianity in the WMAP data: Minkowski functionals and the length of the skeleton," Astrophys. J. **612**, 64 (2004) [arXiv:astro-ph/0401276].

[7] C. Gordon, "Broken Isotropy from a Linear Modulation of the Primordial Perturbations," arXiv:astro-ph/0607423.
E. Komatsu *et al.*, "First Year Wilkinson Microwave Anisotropy Probe (WMAP) Observations: Tests of Gaussianity," Astrophys. J. Suppl. **148**, 119 (2003) [arXiv:astro-ph/0302223].
P. Coles, P. Dineen, J. Earl and D. Wright, "Phase Correlations in Cosmic Microwave Background Temperature Maps," Mon. Not. Roy. Astron. Soc. **350**, 983 (2004) [arXiv:astro-ph/0310252].
P. Mukherjee and Y. Wang, "Wavelets and WMAP non-Gaussianity," Astrophys. J. **613**, 51 (2004) [arXiv:astro-ph/0402602].
K. Land and J. Magueijo, "The axis of evil," Phys. Rev. Lett. **95**, 071301 (2005) [arXiv:astro-ph/0502237].

A. de Oliveira-Costa, M. Tegmark, M. Zaldarriaga and A. Hamilton, "The significance of the largest scale CMB fluctuations in WMAP," Phys. Rev. D **69**, 063516 (2004) [arXiv:astro-ph/0307282].

P. Coles, P. Dineen, J. Earl and D. Wright, "Phase Correlations in Cosmic Microwave Background Temperature Maps," Mon. Not. Roy. Astron. Soc. **350**, 983 (2004) [arXiv:astro-ph/0310252].

D. J. Schwarz, G. D. Starkman, D. Huterer and C. J. Copi, "Is the low-l microwave background cosmic?," Phys. Rev. Lett. **93**, 221301 (2004) [arXiv:astro-ph/0403353].

C. J. Copi, D. Huterer, D. J. Schwarz and G. D. Starkman, "On the large-angle anomalies of the microwave sky," Mon. Not. Roy. Astron. Soc. **367**, 79 (2006) [arXiv:astro-ph/0508047].

C. J. Copi, D. Huterer and G. D. Starkman, "Multipole Vectors–a new representation of the CMB sky and evidence for statistical anisotropy or non-Gaussianity at $2 \leq l \leq 8$," Phys. Rev. D **70**, 043515 (2004) [arXiv:astro-ph/0310511].

Y. Wiaux, P. Vielva, E. Martinez-Gonzalez and P. Vandergheynst, "Global universe anisotropy probed by the alignment of structures in the cosmic microwave background," Phys. Rev. Lett. **96**, 151303 (2006) [arXiv:astro-ph/0603367].

[8] D. L. Larson and B. D. Wandelt, "The Hot and Cold Spots in the WMAP Data are Not Hot and Cold Enough," Astrophys. J. **613**, L85 (2004) [arXiv:astro-ph/0404037].

M. Cruz, E. Martinez-Gonzalez, P. Vielva and L. Cayon, "Detection of a non-Gaussian Spot in WMAP," Mon. Not. Roy. Astron. Soc. **356**, 29 (2005) [arXiv:astro-ph/0405341].

P. Vielva, E. Martinez-Gonzalez, R. B. Barreiro, J. L. Sanz and L. Cayon, "Detection of non-Gaussianity in the WMAP 1-year data using spherical wavelets," Astrophys. J. **609**, 22 (2004) [arXiv:astro-ph/0310273].

[9] H. K. Eriksen, A. J. Banday, K. M. Gorski, F. K. Hansen and P. B. Lilje, "Hemispherical power asymmetry in the three-year Wilkinson Microwave Anisotropy Probe sky maps," arXiv:astro-ph/0701089.

[10] C. Copi, D. Huterer, D. Schwarz and G. Starkman, "The Uncorrelated Universe: Statistical Anisotropy and the Vanishing Angular Correlation Function in WMAP Years 1-3," arXiv:astro-ph/0605135.

T. R. Jaffe, A. J. Banday, H. K. Eriksen, K. M. Gorski and F. K. Hansen, "Evidence of vorticity and shear at large angular scales in the WMAP data: A violation of cosmological isotropy?," Astrophys. J. **629**, L1 (2005) [arXiv:astro-ph/0503213].

K. Land and J. Magueijo, "The Axis of Evil revisited," arXiv:astro-ph/0611518.

[11] F. K. Hansen, A. J. Banday, H. K. Eriksen, K. M. Gorski and P. B. Lilje, "Foreground Subtraction of Cosmic Microwave Background Maps using WI-FIT (Wavelet based hIgh resolution Fitting of Internal Templates)," arXiv:astro-ph/0603308.

[12] D. Maino, S. Donzelli, A. J. Banday, F. Stivoli and C. Baccigalupi, "CMB signal in WMAP 3yr data with FastICA," arXiv:astro-ph/0609228.

[13] C. Raeth, P. Schuecker and A. J. Banday, "A Scaling Index Analysis of the WMAP three year data: Signatures of non-Gaussianities and Asymmetries in the CMB," arXiv:astro-ph/0702163.

[14] J. Hoftuft, H. K. Eriksen, A. J. Banday, K. M. Gorski, F. K. Hansen and P. B. Lilje, "Increasing evidence for hemispherical power asymmetry in the five-year WMAP data," arXiv:0903.1229 [astro-ph.CO].

F. K. Hansen, A. J. Banday, K. M. Gorski, H. K. Eriksen and P. B. Lilje, "Power Asymmetry in Cosmic Microwave Background Fluctuations from Full Sky to Sub-degree Scales: Is the Universe Isotropic?," arXiv:0812.3795 [astro-ph].

[15] A. Hajian, "Analysis of the apparent lack of power in the cosmic microwave background anisotropy at large angular scales," arXiv:astro-ph/0702723.
A. Hajian, T. Souradeep and N. J. Cornish, "Statistical Isotropy of the WMAP Data: A Bipolar Power Spectrum Analysis," Astrophys. J. **618**, L63 (2004) [arXiv:astro-ph/0406354].

[16] E. P. Donoghue and J. F. Donoghue, "Isotropy of the early universe from CMB anisotropies," Phys. Rev. D **71**, 043002 (2005) [arXiv:astro-ph/0411237].

[17] A. E. Gumrukcuoglu, C. R. Contaldi and M. Peloso, arXiv:astro-ph/0608405.
A. E. Gumrukcuoglu, C. R. Contaldi and M. Peloso, JCAP **0711**, 005 (2007) [arXiv:0707.4179 [astro-ph]].

[18] C. Vale, "Local Pancake Defeats Axis of Evil," arXiv:astro-ph/0509039.
R. V. Buniy, "Eccentric inflation and WMAP," Int. J. Mod. Phys. A **20**, 1095 (2005) [arXiv:hep-ph/0408026].
D. Langlois and T. Piran, "Dipole anisotropy from an entropy gradient," Phys. Rev. D **53**, 2908 (1996) [arXiv:astro-ph/9507094].
S. H. S. Alexander, "Is cosmic parity violation responsible for the anomalies in the WMAP data?," arXiv:hep-th/0601034.
K. Land and J. Magueijo, "Template fitting and the large-angle CMB anomalies," [arXiv:astro-ph/0509752].
B. Feng and X. Zhang, "Double inflation and the low CMB quadrupole," Phys. Lett. B **570**, 145 (2003) [arXiv:astro-ph/0305020].
J. Levin, "Topology and the cosmic microwave background," Phys. Rept. **365**, 251 (2002) [arXiv:gr-qc/0108043].
A. de Oliveira-Costa, G. F. Smoot and A. A. Starobinsky, "Can the lack of symmetry in the COBE/DMR maps constrain the topology of the universe?," Astrophys. J. **468**, 457 (1996) [arXiv:astro-ph/9510109].
L. Ackerman, S. M. Carroll and M. B. Wise, "Imprints of a Primordial Preferred Direction on the Microwave Background," arXiv:astro-ph/0701357.
T. Koivisto and D. F. Mota, "Accelerating Cosmologies with an Anisotropic Equation of State," Astrophys. J. **679**, 1 (2008) [arXiv:0707.0279 [astro-ph]].
C. G. Boehmer and D. F. Mota, "CMB Anisotropies and Inflation from Non-Standard Spinors," Phys. Lett. B **663**, 168 (2008) [arXiv:0710.2003 [astro-ph]].
A. L. Erickcek, M. Kamionkowski and S. M. Carroll, Phys. Rev. D **78**, 123520 (2008) [arXiv:0806.0377 [astro-ph]].
A. L. Erickcek, S. M. Carroll and M. Kamionkowski, "Superhorizon Perturbations and the Cosmic Microwave Background," Phys. Rev. D **78**, 083012 (2008) [arXiv:0808.1570 [astro-ph]].
C. Pitrou, T. S. Pereira and J. P. Uzan, "Predictions from an anisotropic inflationary era," JCAP **0804**, 004 (2008) [arXiv:0801.3596 [astro-ph]].
A. R. Pullen and M. Kamionkowski, "Cosmic Microwave Background Statistics for a Direction-Dependent Primordial Power Spectrum," Phys. Rev. D **76**, 103529 (2007) [arXiv:0709.1144 [astro-ph]].
K. Dimopoulos, M. Karciauskas, D. H. Lyth and Y. Rodriguez, "Statistical anisotropy of the curvature perturbation from vector field perturbations," arXiv:0809.1055 [astro-ph].
X. Gao, "Can Relic Superhorizon Inhomogeneities be Responsible for Large-Scale CMB Anomalies?," arXiv:0903.1412 [astro-ph.CO].
Y. Shtanov and H. Pyatkovska, "Statistical anisotropy in the inflationary universe," arXiv:0904.1887 [gr-qc].

[19] J. W. Moffat, "Cosmic Microwave Background, Accelerating Universe and Inhomogeneous Cosmology," JCAP **0510**, 012 (2005) [arXiv:astro-ph/0502110].
C. Gordon, W. Hu, D. Huterer and T. Crawford, "Spontaneous Isotropy Breaking: A Mechanism for CMB Multipole Alignments," [arXiv:astro-ph/0509301].
K. T. Inoue and J. Silk, "Local Voids as the Origin of Large-angle Cosmic Microwave Background Anomalies: The Effect of a Cosmological Constant," arXiv:astro-ph/0612347.

[20] B. A. Powell and W. H. Kinney, "The pre-inflationary vacuum in the cosmic microwave background," arXiv:astro-ph/0612006.
L. Covi, J. Hamann, A. Melchiorri, A. Slosar and I. Sorbera, "Inflation and WMAP three year data: Features have a future!," Phys. Rev. D **74**, 083509 (2006) [arXiv:astro-ph/0606452].
D. Langlois and F. Vernizzi, "From heaviness to lightness during inflation," JCAP **0501**, 002 (2005) [arXiv:astro-ph/0409684].

[21] J. M. Cline, P. Crotty and J. Lesgourgues, "Does the small CMB quadrupole moment suggest new physics?," JCAP **0309**, 010 (2003) [arXiv:astro-ph/0304558].
R. Sinha and T. Souradeep, "Post-WMAP assessment of infrared cutoff in the primordial spectrum from inflation," Phys. Rev. D **74**, 043518 (2006) [arXiv:astro-ph/0511808].

[22] V. Mukhanov, *Physical foundations of cosmology* (Cambridge University Press, 2005).

[23] V. F. Mukhanov, H. A. Feldman and R. H. Brandenberger, "Theory of cosmological perturbations. Part 1. Classical perturbations. Part 2. Quantum theory of perturbations. Part 3. Extensions," Phys. Rept. **215**, 203 (1992).

[24] U. Seljak and M. Zaldarriaga, Astrophys. J. **469**, 437 (1996) [arXiv:astro-ph/9603033], http://www.cmbfast.org/

[25] M. Doran, JCAP **0510**, 011 (2005) [arXiv:astro-ph/0302138], http://www.cmbeasy.org/

[26] A. Lewis, A. Challinor and A. Lasenby, Astrophys. J. **538**, 473 (2000) [arXiv:astro-ph/9911177], http://camb.info/

[27] F. Finelli and A. Gruppuso, arXiv:hep-th/0501089.

[28] G. Hinshaw *et al.* [WMAP Collaboration], "Three-year Wilkinson Microwave Anisotropy Probe (WMAP) observations: Temperature analysis," arXiv:astro-ph/0603451.

[29] R. K. Sachs and A. M. Wolfe, "Perturbations of a cosmological model and angular variations of the microwave background," Astrophys. J. **147**, 73 (1967).

[30] A.R Liddle, D.H Lyth, *Cosmological Inflation and Large-Scale structure* (Cambridge University Press, 2000).